ACS APPLIED MATERIALS & INTERFACES

Research Article

www.acsami.org

Fully Printed, Rapid-Response Sensors Based on Chemically Modified Graphene for Detecting NO_2 at Room Temperature

Lei Huang,* Zhenping Wang, Jiankun Zhang, Jianlong Pu, Youjie Lin, Shuhua Xu, Leo Shen, Qi Chen, and Wangzhou Shi

Joint Lab with Wuhu Token for Graphene Electrical Materials and Application, Department of Physics, Shanghai Normal University, Guilin Road 100, Shanghai 200234, China

Supporting Information

ABSTRACT: Reduced graphene oxide (RGO) has proven to be effective in trace gas detection at room temperature ambient conditions. However, the slow response−recovery characteristic is a major hurdle for the RGO-based gas sensors. Herein, we report a gravure-printed chemoresistor-type NO_2 sensor based on sulfonated RGO (S-RGO) decorated with Ag nanoparticles (Ag−S-RGO). Large amounts of silver nanoparticles with an average particle size of 10−20 nm were uniformly assembled on flat S-RGO surfaces. The printed Ag−S-RGO sensor possesses a high sensitivity and fast response−recovery characteristic over NO_2 concentrations ranging from 0.5 to 50 ppm. Upon exposure to 50 ppm NO_2 at room temperature, the Ag−S-RGO sensor shows a sensitivity of 74.6%, a response time of 12 s and a recovery time of 20 s. In addition, the Ag−S-RGO sensors exhibit satisfactory flexibility with an almost constant resistance after 1000 bending cycles. The printed and high-performance Ag−S-RGO sensors described here will be a good prospect in environmental monitoring of NO_2.

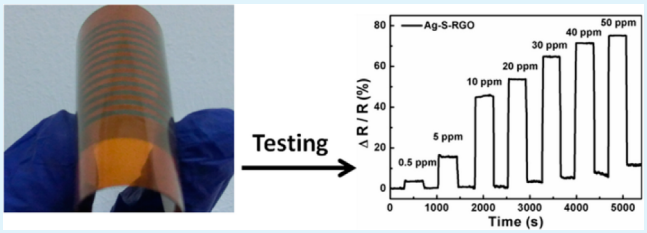

KEYWORDS: *printed sensor, reduced graphene oxide, Ag nanoparticles, nanocomposite structure*

1. INTRODUCTION

With the demand of real-time analysis of gaseous chemical analytes for environmental monitoring, the development of printed gas sensors on flexible substrates is ongoing for wireless sensor applications.[1−3] Functionalized graphene holds exceptional promise for chemical sensors due to its large specific surface and high carrier mobility.[4,5] Furthermore, the unique structure of graphene endows a high sensitivity of resistance to small changes in environmental conditions,[6] and the ability to print graphene sheets with chemical modification enables fabrication of selective gas sensors.[3,4] It has been demonstrated that graphene-based sensors can detect trace amounts of different gases including NO_2, NH_3, H_2O and CO.[7,8] Among the gases, the graphene devices exhibit the best performance for detecting the NO_2 molecules based on previous studies both from the first-principles calculations and experiments.[8,9] In addition, NO_2 is very harmful to human beings and threatens environmental security due to its role as a source of photochemical smog and acid rain.[10] Therefore, the detection of NO_2 gas is of significant interest in environmental monitoring.

Since the pioneer research on detection of single NO_2 molecule by using mechanically exfoliated graphene sheets,[8] multiple research groups have exploited reduced graphene oxide (RGO)-based NO_2 sensors with the goal of optimizing various characteristics by utilizing its possibility for chemical modifications.[3,6,11−13] However, RGO devices are generally not fully recovered at ambient conditions due to gaseous molecular interactions with higher energy binding sites, such as structural defects and oxygen functional groups.[11] Chemical modification with foreign groups or atoms is an effective approach to intrinsically change surface properties of RGO.[14−18] Shi et al. demonstrated that modificated RGO with sulfophenyl (−SO_3H) could improve the recoverability performance of RGO for detection of NO_2.[19] However, long response−recovery times hindered their use as stand-alone sensing elements. Recently, assembly of metal (e.g., Ag, Au and Te) nanoparticles (NPs) into carbon nanotube (CNT) or RGO sheets can be exploited to enhance sensing performance of chemoresistor-type devices.[20−22] It has been demonstrated that CNTs coated with Ag NPs not only promoted the sensitivity to NO_2 but also shortened the response time from 244 to 77 s.[23] Tjoa and co-workers found that the RGO decorated with gold and silver NPs caused a potential drop at the metal NP−graphene interface, and the NPs were effective sites for gas interaction, improving the sensitivity to NO_2.[24] However, the gas sensing performance of the NP-RGO has not been improved significantly in their work because the decorating of metal NPs on the surface of RGO could be efficiently inhibited due to the aggregation and restacking of RGO. Therefore, the stabilization of RGO nanosheets in aqueous dispersion is an important premise for RGO decorated with metal NPs.

Received: February 9, 2014
Accepted: May 7, 2014
Published: May 7, 2014

Solution-phase RGO offers significant advantages for scalability and compatibility with additive printing techniques.[25,26] Among printing techniques, the use of gravure printing of sensor devices is particularly attractive due to its high throughput, optimal control of sensing layer thickness and ability to use a wide range of inks.[27]

Herein, we present a flexible chemoresistor-type NO_2 sensor based on the sulfonated RGO (S-RGO) decorated with Ag nanoparticles (Ag–S-RGO), which was printed onto a polyimide (PI) substrate by a gravure printing technique. The Ag–S-RGO inks were prepared by a simple wet-chemical pathway using graphite oxide (GO), sulfanilic acid and silver nitrate ($AgNO_3$) as starting materials. By successively printing Ag interdigitated electrodes (Ag-IDEs) and the Ag–S-RGO sensing layer on the PI substrate, the Ag–S-RGO sensor was fabricated (Scheme 1). Because of the chemical modification of RGO with $-SO_3H$ groups and Ag NPs, the printed Ag–S-RGO sensor exhibits a high sensitivity and fast response–recovery characteristic to NO_2 at room temperature.

Scheme 1. (a) Photographs of Ag–S-RGO Ink and Ag–S-RGO Sensing Layer Printed onto the PI Substrate with Ag-IDEs, Respectively; (b) Schematic of the Printed Ag–S-RGO Sensor

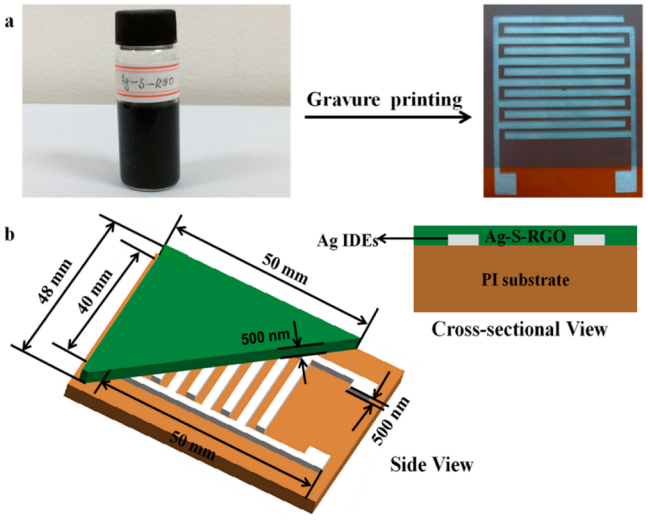

2. EXPERIMENTAL SECTION

2.1. Preparation of S-RGO. GO sheets were synthesized by the chemical oxidation of natural graphite flakes (Alfa-Aesar) using the Hummers method as described previously.[28,29] S-RGO was prepared from GO through aryl diazonium reaction of sulfanilic acid.[19,30] 150 mg of GO was dispersed in 150 mL of deionized (DI) water via a mild sonication treatment to get a brown GO dispersion. A 5 wt % sodium carbonate solution was added into the GO dispersion until its pH value was adjusted to 10. Then, 15 mL (40 mg/mL) of sodium borohydride was mixed with the GO dispersion at 80 °C with stirring for 1 h. The prereduced GO was centrifuged and rinsed thoroughly with DI water until the pH was about 7. Subsequently, it was redispersed in 150 mL of water with a sonication for 30 min. At ice cooled conditions, 184 mg of sulfanilic acid and 72 mg of sodium nitrite were reacted with HCl (40 mL, 0.05 M) to form the aryl diazonium salt. Then, the diazonium salt was dispersed in the prereduced RGO dispersion and kept at 0 °C for 2 h to obtain the S-RGO product. The S-RGO was further purified by washing with DI water five times and redispersed into 150 mL of DI water.

2.2. Preparation of Ag–S-RGO Inks. A solution of 300 mg of $AgNO_3$ in 30 mL of DI water was added into the S-RGO solution at 50 °C with stirring for 2 h. Then, 25 μL of hydrazine (50%) was added into the above solution and the mixture was kept at 100 °C with stirring for 24 h to obtain the Ag–S-RGO product. The Ag–S-RGO was further centrifuged and rinsed with DI water several times. The resulting solid was mixed with 20 mL of DI water/ethanol (1:9, volume ratio) to get Ag–S-RGO inks.

2.3. Fabrication of Fully Printed Ag–S-RGO NO_2 Sensors. The polyimide (PI) substrates were cleaned with deionized water by ultrasonication. Then, the substrates were placed in a reaction ion etching system (RIE-200NL, Samco) exposed to O_2 plasma for 20 s with the following etching parameters (RF power 100 W, O_2 gas flow 80 sccm, gas pressure 10 Pa). The printing experiments were performed by a gravure printer (Schläfli Labratester) at room temperature. The 500 nm thick Ag-IDEs with the dimensions of 40 × 50 mm (Scheme 1b) was made by gravure printing and dried at 120 °C for 1 h. Subsequently, the Ag–S-RGO sensing layer was printed directly on the prepatterned Ag-IDEs and dried at 80 °C for 0.5 h.

2.4. Characterization. The morphology and chemical composition mapping through energy-dispersive spectroscopy (EDS) of the Ag–S-RGO hybrids was examined by field emission scanning electron microscopy (FE-SEM, JSM-7000F) and transmission electron microscopy (TEM, JEM2010-HR). Raman analysis (Jobin Yvon LabRam-010, with a laser excitation wavelength of 632.8 nm and a spot size of 1 μm^2) was performed to measure the Ag–S-RGO hybrids. XRD was recorded on a Bruker D8-Focus X-ray diffractometer (40 kV, 40 mA) in the 2θ range of 10°–80° at a scanning rate of 0.5° min^{-1}. Elemental composition analysis was

Scheme 2. Illustration for the Preparation of Ag–S-RGO

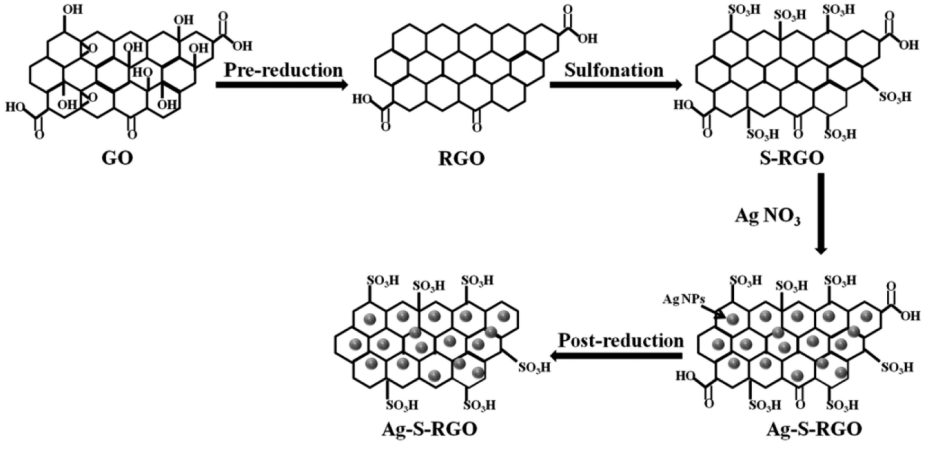

dx.doi.org/10.1021/am500843p | ACS Appl. Mater. Interfaces 2014, 6, 7426–7433

carried out using X-ray photoelectron spectroscopy (XPS, PHI 5000 Versa Probe).

2.5. Sensor Measurements. The gas sensing experiments were carried out in a homemade sensor testing system (EE-12b, a cylindrical stainless steel chamber with a size of 12 L). A certain amount of NO_2 is injected into the testing chamber. The NO_2 concentration in the chamber can be calculated based on the injected amount. The interaction between sensors with NO_2 brings the change of the conductance, which is recorded by a high-resistance meter (Keithley, 6517B). Then, the upper lid of the chamber is opened for the sensor recovery.

All the measurements were carried out in the ambient air (25 °C, 30% relative humidity). The sensor response (S) was calculated by the following equation:

$$S(\%) = \frac{R - R_g}{R} \times 100 = \frac{\Delta R}{R} \times 100 \quad (1)$$

where R_{gas} (R_g) and R are the electrical resistances of the sensor in the tested gas and air, respectively. Herein, the response time is defined as the time taken for the sensor output to reach 90% of its steady value. The recovery time is the time for the resistance in equilibrium to go down to 10% of the initial value in air since the test gas is released.

3. RESULTS AND DISCUSSION

3.1. Preparation and Characterization of Printed Ag−S-RGO Sensor. As outlined in Scheme 2, the Ag−S-RGO inks were synthesized via a wet-chemical pathway including four procedures: (a) prereduction of GO with sodium borohydride; (b) sulfonation RGO via aryl diazonium salt; (c) $AgNO_3$ mixtured with S-RGO; (d) postreduction with hydrazine. It has been demonstrated that the prereduction of GO creates new sp^2 clusters and increases domains size of sp^2 carbon, giving rise to $-SO_3H$ doping effects.[30] Furthermore, the added $-SO_3H$ groups are on the edges of the RGO sheets, rather than in the flat planes, ensuring the minimum damage to graphene structure.[31] In addition, the $-SO_3H$ group is a stronger H-bonding group, which could promote water absorption though a hydrogen bond, making the RGO more hydrophilic. Actually, the presence of negatively charged $-SO_3^-$ units not only imparts sufficient electrostatic repulsion to keep S-RGO sheets separated but also greatly enhances the Ag^+ anchored onto the S-RGO sheets.

The FESEM image in Figure 1a shows that the sheets of Ag−S-RGO are large size and few wrinkled. Especially, large amounts of Ag NPs are uniformly assembled on the S-RGO surfaces. The result is different from the most previous studies, which showed that Ag NPs were capped in the RGO network.[24,32] The TEM image in Figure 1b proves that the Ag NPs were successfully decorated on the S-RGO surfaces. The diameter of Ag NPs ranges from 10 to 20 nm. On the basis of the chemical composition mapping of the Ag−S-RGO as shown in Figure S-1 (Supporting Information), it is indicated that Ag NPs are well-dispersed over the whole RGO sheets, and further confirms the percentages of Ag (Figure 1c) and S (Figure 1d) elements in Ag−S-RGO are 8.76% and 3.43%, respectively.

The comparative Raman spectra of S-RGO and Ag−S-RGO hybrids are shown in Figure 2a. The S-RGO exhibits two characteristic peaks, corresponding to the D and G bands. D band at 1340 cm^{-1} signified lattice disorder is associated with the breathing mode of k-point photons of A_{1g} symmetry and G band near 1623 cm^{-1} implied sp^2 hybridized carbon domains arises due to the E_{2g}-vibration mode.[33] The intensity of the D and G bands for the Ag−S-RGO hybrids increase obviously in comparison to the bare S-RGO hybrids in the same test

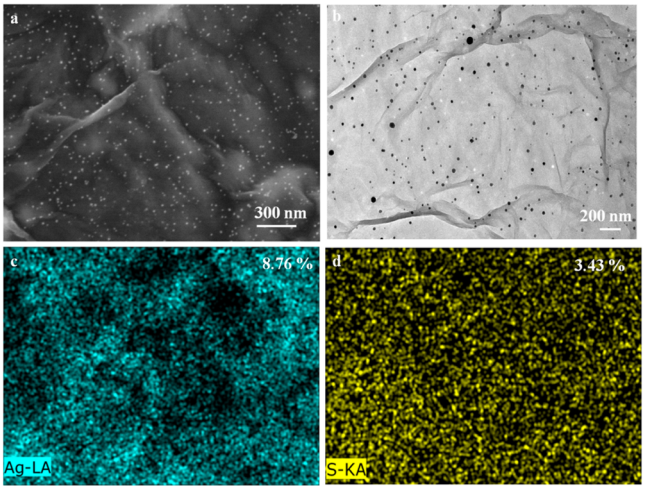

Figure 1. (a) FESEM image of Ag−S-RGO; (b) TEM image of Ag nanoparticles on S-RGO sheets; (c, d) the EDS mapping for Ag (blue) and S (yellow) elements present in Ag−S-RGO.

conditions. The phenomenon may be ascribed to the formation of charge-transfer complexes between Ag NPs and S-RGO. When S-RGO is in contact with Ag NPs, the Ag NPs acquires electron density as S-RGO's Fermi level is closer to the valence band.[34] Such interactions can absorb light at the excitation frequency, consequently producing the surface-enhanced Raman scattering (SERS) effect. It is noted that the strong SERS signal of the Ag−S-RGO hybrids depends on the excitation of surface plasmons, which is tuned by the Ag NP parameters.[35]As mentioned earlier, coupled with flat morphology and hydrophilic surface property, S-RGO sheets have been used as effective absorbents for small size and considerable Ag NPs through electrostatic bonding or $\pi-\pi$ cooperative interactions.

XRD patterns are used to analyze the crystal structure of S-RGO and Ag−S-RGO hybrids in Figure 2b. The S-RGO exhibits a strong diffraction peak at 23.55°, which is attributed to the diffraction from the (002) plane of the hexagonal graphite structure. Its intensity means the degree of graphitisation of the S-RGO. After Ag NPs deposit on the S-RGO surface, this weak peak is shifted to 18.08°, indicating that the assembled Ag NPs slightly increase the interlayer distance. In addition, the Ag−S-RGO hybrids show four diffraction peaks at 2θ = 38.31°, 44.50°, 64.56° and 77.51°, which are attributed to the (111), (200), (220) and (311) planes of Ag NPs with the face-centered cubic (fcc) structure.

XPS is used to analyze surface elemental compositions and their chemical structure of the S-RGO and Ag−S-RGO hybrids in Figure 3a. From both spectra, it can be clearly observed the sharp peaks at 282 and 529 eV correspond to the C 1s and O 1s peaks, respectively. These spectra also present S element at 168 eV. Furthermore, from the high-resolution scan in the inset, it is found that for the different binding energies for S, the peak at 161.7 eV is attributed to the $-SO_3H$ and the broad peak at 168.4 eV is assigned to the high oxidized S originating from H_2SO_4.[36] The survey of Ag−S-RGO hybrids also exhibits Ag peaks, suggesting that the covalent functionalization of S-RGO by $AgNO_3$ is achieved. Figure 3b exhibits the C 1s XPS spectra of S-RGO, which has three main peaks at 284.8, 286.7 and 288.6 eV corresponding to the C—C, C—O and C═O species, respectively. For Ag−S-RGO hybrids (Figure 3c), the intensity of the peaks assigned to both C—O and C═O

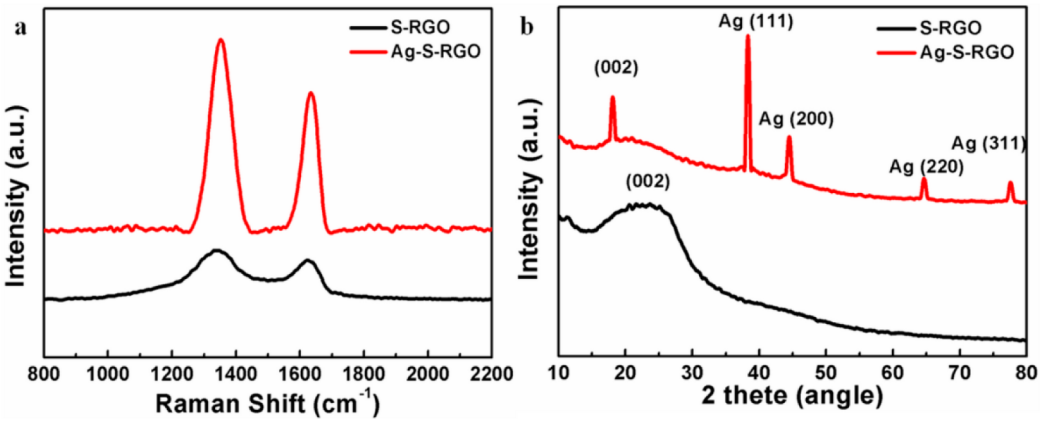

Figure 2. (a) Raman spectra of S-RGO and Ag–S-RGO. (b) XRD patterns of S-RGO and Ag–S-RGO.

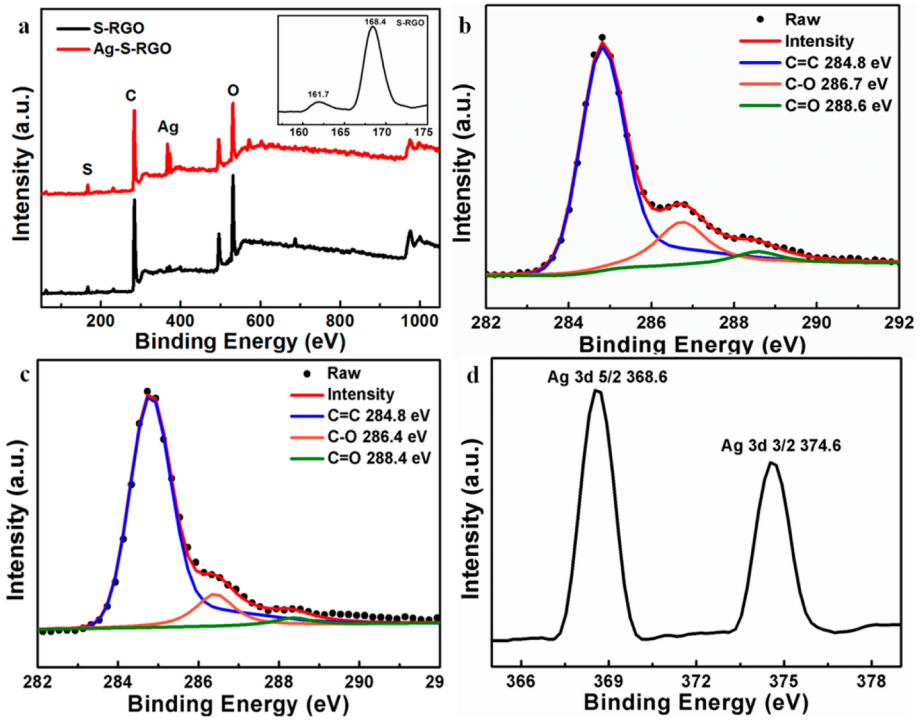

Figure 3. (a) XPS spectra for S-RGO and Ag–S-RGO (inset: the high-resolution curves of the S 2p peaks). (b, c) C 1s XPS spectra for S-RGO and Ag–S-RGO. (d) Ag 3d XPS spectrum of Ag–S-RGO.

groups decreases slightly. The signature of Ag 3d doublet for Ag NPs is shown in Figure 3d. The Ag $3d_{5/2}$ and Ag $3d_{3/2}$ binding energies appear at 368.6 and 374.6 eV, respectively.

3.2. Gas Sensing Properties. The gas sensing measurements of the fully printed Ag–S-RGO sensor were carried out in ambient air (25 °C, 30% relative humidity). Figure 4a displays the normalized change in Ag–S-RGO resistance ($\Delta R/R$) as a function of time for different concentrations of NO_2 ranging from 500 ppb up to 50 ppm. It can be observed that $\Delta R/R$ of the Ag–S-RGO device increases from 3.4% for 500 ppb to 74.6% for 50 ppm of NO_2. The measured resistances of the Ag–S-RGO films decrease upon exposure to oxidizing NO_2 gas. This result is expected because the oxidizing analyte NO_2 withdraws electrons from the *p*-type Ag–S-RGO surface and induces the decrease in electrical resistance.

The response–recovery characteristics of the Ag–S-RGO sensors are shown in Figure 4b,c. A very short response time of 12 s and a quick recovery within 20 s are achieved with an NO_2 concentration of 50 ppm. It can be seen that the fast response–recovery characteristics are almost unchanged at all the concentrations of NO_2. These phenomena are different from the NO_2 sensors based on S-RGO, which have a long response and recovery time of even more than 10 min.[19] The fast response–recovery characteristics of the Ag–S-RGO sensor is mainly attributed to chemical modification of $-SO_3H$ and Ag NPs.

To demonstrate the repeatability of the printed Ag–S-RGO devices, the Ag–S-RGO sensor is exposed to 50 ppm NO_2 at room temperature for five successive cycles. A stable sensing signal with a response of about 71% is observed in Figure 4d. The gas selectivity of the Ag–S-RGO sensor through comparing the sensitivities toward various gases is studied in Figure 5. The response of Ag–S-RGO sensor to 100 ppm NO_2, 1 mL of NH_3, methanol, ethanol and toluene are 90, 101, 5, 4, and 10. It is noted that the electrical resistance of the sensor is increased by exposure to NH_3 gas, which is in the opposite

dx.doi.org/10.1021/am500843p | ACS Appl. Mater. Interfaces 2014, 6, 7426–7433

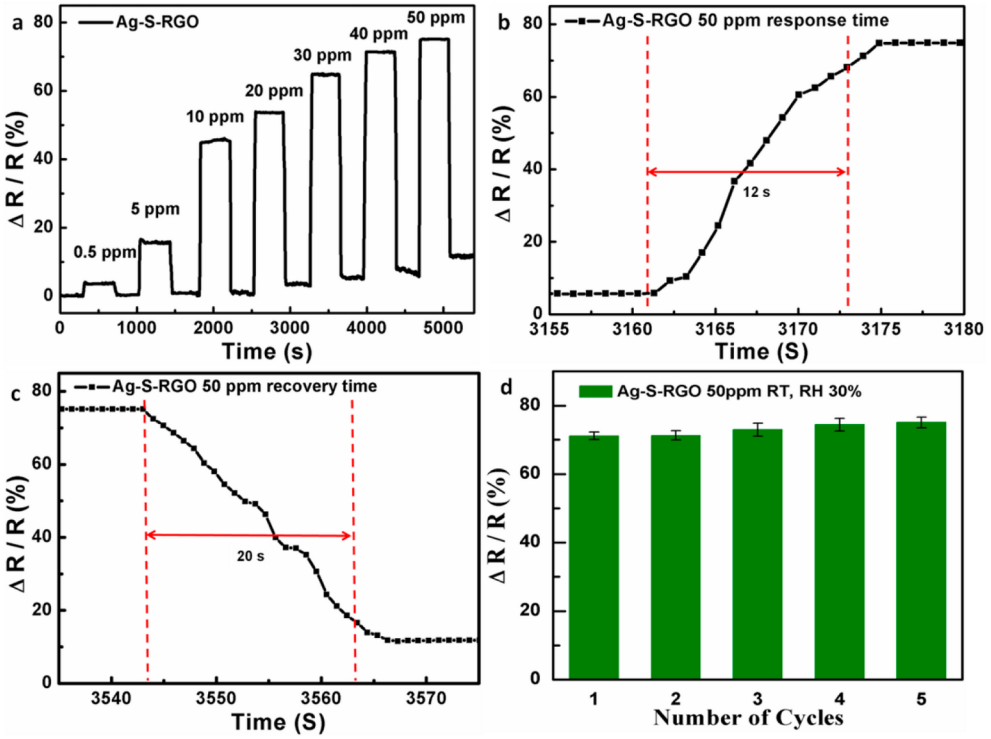

Figure 4. (a) Response of the Ag−S-RGO sensor as a function of time (s) in various concentrations of NO_2 gas. (b, c) Response and recovery times of the Ag−S-RGO sensor. (d) Response of the Ag−S-RGO sensor as a function of time for detection of 50 ppm of NO_2 in five cycles.

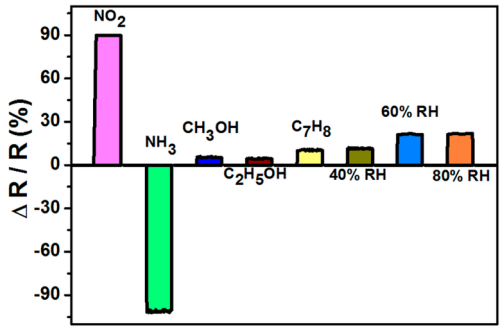

Figure 5. Printed Ag−S-RGO sensing to 100 ppm NO_2, 1 mL (13 ppt) of NH_3, 1 mL (46 ppt) of methanol, 1 mL (32 ppt) of ethanol, 1 mL (18 ppt) of toluene, 40% RH, 60% RH, 80% RH.

direction to NO_2. For NO_2 oxidizing gas, it attracts electrons from the *p*-type Ag−S-RGO, increasing the number of conducting holes, which induces an increase in conductance. On the contrary, NH_3 is a reducing agent that injects electrons into *p*-type Ag−S-RGO and decreases the number of holes, leading to reduced conductance. Humidity is an important factor that might impact the gas sensing properties of graphene.[37] Figure 5 also exhibits the effect of humidity on the sensing characteristics of Ag−S-RGO in the range of 40−80% relative humidity (RH). The Ag−S-RGO sensing response to 40, 60 and 80% RH are 11, 21 and 21, meaning that the different RH has less influence on the printed Ag−S-RGO sensor for detection of NO_2.

A comparison between the sensing performances of the printed Ag−S-RGO sensors and literature reports for NO_2 detection is summarized in Table 1.[11,12,19,24,38] It can be observed that the fully printed Ag−S-RGO sensor has the fastest response−recovery among the graphene-based NO_2 sensors. However, there are other inorganic materials based NO_2 sensors with faster response−recovery characteristic. For example, the In_2O_3 nanowire NO_2 sensor presented a response time as short as 5 s, but the recovery time of the sensor was 30 s by illuminating the sensor with UV light in vacuum.[39] Xiong and co-workers demonstrated the response and recovery time of solid-state $CuO/CuCr_2O_4$ NO_2 sensor was 8 and 10 s, but the working temperature was above 600 °C.[40] In short, the fast response−recovery characteristic of Ag−S-RGO NO_2 sensor can be presented only at room temperature in this work.

RGO is a typical *p*-type semiconductor and the modified RGO with $-SO_3H$ and Ag NPs lead RGO sheets to be further *p*-doped. The gas-sensing mechanism of Ag−S-RGO belongs to surface-controlled type in which the adsorption of atmospheric

Table 1. Graphene-based Sensors for NO_2 Detection

materials	NO_2 concentration (ppm)	work temperature	sensitivity	response time	recovery time
RGO[11]	100 (air)	RT	R_a/R_g = 9.15	15 min	20 min
flexible RGO[12]	5 (air)	RT	$(R_a - R_g)/R_a$ = 12%	7 min	28 min
S-RGO[19]	20 (air)	RT	G_g/G_0 = 7.4	10 min	30 min
Au/Ag-RGO[24]	2 (air)	RT	$(I_g - I_0)/I_0$ = 50%	200 s	200 s
nanoporous RGO[38]	100 (air)	RT	I_g/I_0 = 5	200−300 s	300 s
Ag−S-RGO[Our work]	50 (air)	RT	$(R_a - R_g)/R_a$ = 45%	12 s	20 s

dx.doi.org/10.1021/am500843p | ACS Appl. Mater. Interfaces 2014, 6, 7426−7433

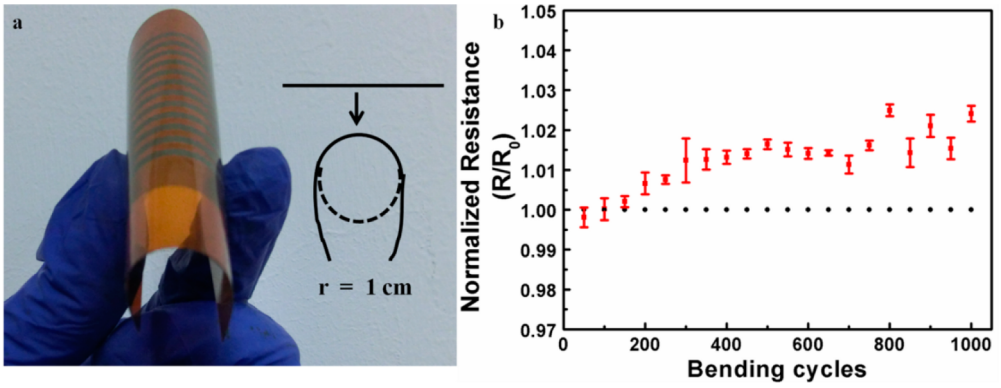

Figure 6. (a) Photograph of a printed Ag−S-RGO sensor and schematics showing the mechanical bend test conditions. (b) Changes of the normalized resistance during the bend test for the Ag−S-RGO sensor.

oxygen and NO_2 molecules on the Ag−S-RGO surface play an important role. In ambient air, oxygen molecules adsorb electrons from the conduction band of the sensing Ag−S-RGO to generate chemisorbed oxygen species O_2^-.[41] When the Ag−S-RGO sensor is exposed to NO_2, the NO_2 molecules can not only capture the electrons from Ag−S-RGO conductance band due to its higher electrophilic property but also react with the absorbed oxygen ion leading to the formation of absorbed NO_2^-.[42] Such adsorption and reaction can capture the electrons from the *p*-type Ag−S-RGO nanosheets, resulting in an increase of the carrier concentration, which eventually increase the conductivity of the sensor. When NO_2 gas flow is stopped, NO_2^-(ads) ions are desorbed (see eq 6). Consequently, a recovery of the initial condition takes place. The process can be expressed in the following reactions:

$$O_2(gas) \rightarrow O_2(ads) \quad (2)$$

$$O_2(ads) + e^- \rightarrow O_2^-(ads) \quad (3)$$

$$NO_2(gas) + e^- \leftrightarrow NO_2^-(ads) \quad (4)$$

$$NO_2(gas) + O_2^-(ads) + 2e^- \leftrightarrow NO_2^-(ads) + 2O^-(ads) \quad (5)$$

$$NO_2^-(ads) + 2O^-(ads) + e^- \rightarrow NO_2(gas) + 2O^{2-}(ads) \quad (6)$$

The superior performance of the Ag−S-RGO-based NO_2 sensor is attributed to the chemical modification of RGO with $-SO_3H$ groups and Ag NPs. The anchored $-SO_3H$ groups make the Ag−S-RGO sheets flat and large, which provides the greatest possible surface area per unit volume. The $-SO_3H$ is an electron-withdrawing group and has many lone pairs of electrons.[16] Gas molecules can be facile desorbed from the Ag−S-RGO sensitive layers due to the weak combination of the gas molecules and the lone-pair electrons in $-SO_3H$ groups. Additionally, the introduction Ag NPs into the S-RGO hybrids can greatly shorten the gas response and recovery time, which is mainly related to the catalytic performance of the Ag NPs. On the one hand, the NO_2 gas is activated and dissociated to NO_2^- by the Ag NPs. The atomic products diffuse to the Ag−S-RGO surface according to the spillover effect.[43] Then the reaction between NO_2 or NO_2^- and the negatively charged oxygen adsorbates (O_2^- or O^-) induces a concentration change of adsorbed oxygen and hence charge transfer. On the other hand, once oxygen adsorbs on the surface of Ag−S-RGO, a charge-depletion layer forms around the Ag NPs. The surface electronic state change of the Ag NPs induces a fast change in resistance of Ag−S-RGO.

We also investigate the flexibility of fully printed Ag−S-RGO sensors by measuring their electrical resistance as a function of bending cycles. Figure 6a shows a photograph of the fully printed Ag−S-RGO sensor. The R_n/R_0 ratio, where R_0 is the initial resistance and R_n is the resistance measured when flattened after a certain number of bending cycles, shows a small increase (Figure 6b). After 1000 cycles for a bend radius of 1 cm, the R_n/R_0 ratio only increases to 1.025. The result shows the excellent electromechanical stability of the fully printed Ag−S-RGO sensors on a PI substrate.

4. CONCLUSION

We have demonstrated the effectiveness of the fully printed Ag−S-RGO sensors for the high sensitivity detection of NO_2 at room temperature. Compared with other graphene-based sensors, the response and recovery time of the Ag−S-RGO sensor is only 12 and 20 s, respectively. The sensing properties of the Ag−S-RGO sensor also exhibit excellent stability and wet-tolerance. The superior performances of the Ag−S-RGO sensor are attributed to the chemical modification of RGO with $-SO_3H$ groups and Ag NPs. In addition, the printed Ag−S-RGO device is mechanically robust, flexible and can be handled easily. Thus, the fully printed, lightweight and high-performance NO_2 sensors described here may be deployed for real-time environmental monitoring.

■ ASSOCIATED CONTENT

Ⓢ Supporting Information

Translation calculation from 1 mL of ammonia, methanol, ethanol and toluene to the concentration of the gases, and the full EDS mapping of C, O, Ag and S for Ag−S-RGO. This material is available free of charge via the Internet at http://pubs.acs.org.

■ AUTHOR INFORMATION

Corresponding Author

*L. Huang. E-mail: leihuang@shnu.edu.cn; elhuang68@yahoo.com.sg. Tel.: +86 21 6432 8968. Fax: +86 21 6432 8968.

Notes

The authors declare no competing financial interest.

■ ACKNOWLEDGMENTS

This research was supported by the National Natural Science Foundation of China (No. 50972091), the Shanghai Municipal

Science & Technology Commission key supporting project (No. 12120502900), Shanghai Municipal Education Committee Key Laboratory of Molecular Imaging Probes and Sensors, industrial research fund from Wuhu Token Sciences Co., Ltd. Prof. Lei Huang appreciates the support of The Program for Professor of Special Appointment (Eastern Scholar) at Shanghai Institutions of Higher Learning.

REFERENCES

(1) Fan, Z.; Ho, J.; Takahashi, T.; Yerushalmi, R.; Takei, K.; Ford, A.; Chueh, Y. L.; Javey, A. Toward the Development of Printable Nanowire Electronics and Sensors. *Adv. Mater.* **2009**, *21*, 3730−3743.

(2) Ammu, S.; Dua, V.; Agnihotra, S. R.; Surwade, S.; Phulgirkar, A.; Patel, S.; Manohar, S. Flexible, All-Organic Chemiresistor for Detecting Chemically Aggressive Vapors. *J. Am. Chem. Soc.* **2012**, *134*, 4553−4556.

(3) Dua, V.; Surwade, S.; Ammu, S.; Agnihotra, S. R.; Jain, S.; Roberts, K.; Park, S.; Ruoff, R.; Manohar, S. All-Organic Vapor Sensor Using Inkjet-Printed Reduced Graphene Oxide. *Angew. Chem., Int. Ed.* **2010**, *49*, 2154−2157.

(4) Wang, S.; Ang, P. K.; Wang, Z.; Tang, A. L. L.; Thong, J. L.; Loh, K. P. High Mobility, Printable, and Solution-Processed Graphene Electronics. *Nano Lett.* **2010**, *10*, 92−98.

(5) Pal, A.; Ghatak, N. S.; Kochat, V.; Sneha, E. S.; Sampathkumar, A.; Raghavan, S.; Ghosh, A. Microscopic Mechanism of 1/f Noise in Graphene: Role of Energy Band Dispersion. *ACS Nano* **2011**, *3*, 2075−2081.

(6) Lu, G. H.; Ocola, L.; Chen, J. H. Gas Detection Using Low-Temperature Reduced Graphene Oxide Sheets. *Appl. Phys. Lett.* **2009**, *94*, 083111−08313.

(7) Joshi, R.; Gomez, H.; Alvi, F.; Kumar, A. Graphene Films and Ribbons for Sensing of O_2, and 100 ppm of CO and NO_2 in Practical Conditions. *J. Phys. Chem. C* **2010**, *114*, 6610−6613.

(8) Schedin, F.; Geim, A. K.; Morozov, S. V.; Hill, E. W.; Blake, P.; Katsnelson, M. I.; Novoselov, K. S. Detection of Individual Gas Molecules Adsorbed on Graphene. *Nat. Mater.* **2007**, *6*, 652−655.

(9) Lin, X.; Ni, J.; Fang, C. Adsorption Capacity of H_2O, NH_3, CO, and NO_2 on the Pristine Graphene. *J. Appl. Phys.* **2013**, *113*, 034306−034312.

(10) Hoek, G.; Brunekreef, B.; Fischer, P.; Wijnen, J. The Association between Air Pollution and Heart Failure, Arrhythmia, Embolism, Thrombosis, and Other Cardiovascular Causes of Death in a Time Series Study Gerard Hoek. *Epidemiology* **2001**, *12*, 355−357.

(11) Lu, G.; Park, S.; Yu, K.; Ruoff, R. S.; Ocola, L.; Rosenmann, D.; Chen, J. Toward Practical Gas Sensing with Highly Reduced Graphene Oxide: A New Signal Processing Method To Circumvent Run-to-Run and Device-to-Device Variations. *ACS Nano* **2011**, *5*, 1154−1165.

(12) Su, P. G.; Shieh, H. C. Flexible NO_2 Sensors Fabricated by Layer-by-Layer Covalent Anchoring and in Situ Reduction of Graphene Oxide. *Sens. Actuators, B* **2014**, *190*, 865−872.

(13) Mao, S.; Yu, K.; Cui, S.; Bo, Z.; Lu, G.; Chen, J. A New Reducing Agent to Prepare Single-Layer, High-Quality Reduced Graphene Oxide for Device Applications. *Nanoscale* **2011**, *3*, 2849−2853.

(14) Nethravathi, C.; Rajamathi, M. Chemically Modified Graphene Sheets Produced by the Solvothermal Reduction of Colloidal Dispersions of Graphite Oxide. *Carbon* **2008**, *46*, 1994−1998.

(15) Longun, J.; Walker, G.; Iroh, J. O. Surface and Mechanical Properties of Graphene−Clay/Polyimide Composites and Thin Films. *Carbon* **2013**, *63*, 9−22.

(16) Zhang, H.; Feng, J.; Fei, T.; Liu, S.; Zhang, T. SnO_2 Nanoparticles-Reduced Graphene Oxide Nanocomposites for NO_2 sensing at Low Operating Temperature. *Sens. Actuators, B* **2014**, *190*, 472−478.

(17) Liu, S.; Tian, J.; Wang, L.; Sun, X. A Method for the Production of Reduced Graphene Oxide Using Benzylamine as a Reducing and Stabilizing Agent and its Subsequent Decoration with Ag Nanoparticles for Enzymeless Hydrogen Peroxide Detection. *Carbon* **2011**, *49*, 3158−3164.

(18) Liu, S.; Tian, J.; Wang, L.; Li, H.; Zhang, Y.; Sun, X. Stable Aqueous Dispersion of Graphene Nanosheets: Noncovalent Functionalization by a Polymeric Reducing Agent and Their Subsequent Decoration with Ag Nanoparticles for Enzymeless Hydrogen Peroxide Detection. *Macromolecules* **2010**, *43*, 10078−10083.

(19) Yuan, W.; Liu, A.; Huang, L.; Li, C.; Shi, G. High-Performance NO_2 Sensors Based on Chemically Modified Graphene. *Adv. Mater.* **2012**, *25*, 766−771.

(20) Yu, H.; Xu, P.; Lee, D. W.; Li, X. Porous-Layered Stack of Functionalized AuNP−rGO (Gold Nanoparticles−Reduced Graphene Oxide) Nanosheets as a Sensing Material for the Micro-Gravimetric Detection of Chemical Vapor. *J. Mater. Chem. A* **2013**, *1*, 4444−4450.

(21) Zanolli, Z.; Leghrib, R.; Felten, A.; Pireaux, J. J.; Liobet, E.; Charlier, J. C. Gas Sensing with Au-Decorated Carbon Nanotubes. *ACS Nano* **2011**, *4*, 4592−4599.

(22) Zhang, M.; Su, H. C.; Rheem, Y.; Hangarter, C. M.; Myung, N. V. A Rapid Room-Temperature NO_2 Sensor Based on Tellurium−SWNT Hybrid Nanostructures. *J. Phys. Chem. C* **2012**, *116*, 20067−20074.

(23) Cui, S.; Pu, H.; Mattson, E. C.; Lu, G.; Mao, S.; Weinert, M.; Hirschmugl, C.; Josifovska, M. G.; Chen, J. Ag Nanocrystal as a Promoter for Carbon Nanotube-Based Room-Temperature Gas Sensors. *Nanoscale* **2012**, *4*, 5887−5894.

(24) Tjoa, V.; Jun, W.; Dravid, V.; Mhaisalkar, S.; Mathews, N. Hybrid Graphene−Metal Nanoparticle Systems: Electronic Properties and Gas Interaction. *J. Mater. Chem.* **2011**, *21*, 15593−15599.

(25) Shin, K. Y.; Hong, J. Y.; Jang, J. Micropatterning of Graphene Sheets by Inkjet Printing and Its Wideband Dipole-Antenna Application. *Adv. Mater.* **2011**, *23*, 2113−2118.

(26) Tölle, F. J.; Fabritius, M.; Mülhaupt, R. Emulsifier-Free Graphene Dispersions with High Graphene Content for Printed Electronics and Freestanding Graphene Films. *Adv. Funct. Mater.* **2012**, *22*, 1136−1144.

(27) Tobjörk, D.; Österbacka, R. Paper Electronics. *Adv. Mater.* **2011**, *23*, 1935−1961.

(28) Huang, L.; Liu, Y.; Ji, L. C.; Xie, Y. Q.; Wang, T.; Shi, W. Z. Pulsed Laser Assisted Reduction of Graphene Oxide. *Carbon* **2011**, *49*, 2431−2436.

(29) Hummers, W. S.; Offeman, R. E. Preparation of Graphitic Oxide. *J. Am. Chem. Soc.* **1958**, *80*, 1339.

(30) Si, Y. C.; Samulski, E. Synthesis of Water Soluble Graphene. *Nano Lett.* **2008**, *8*, 1679−1682.

(31) Zhao, G.; Jiang, L.; He, Y.; Li, J.; Dong, H.; Wang, X.; Hu, W. Sulfonated Graphene for Persistent Aromatic Pollutant Management. *Adv. Mater.* **2011**, *23*, 3959−3963.

(32) Lu, L.; Liu, J.; Hu, Y.; Zhang, Y.; Chen, W. Graphene-Stabilized Silver Nanoparticle Electrochemical Electrode for Actuator Design. *Adv. Mater.* **2013**, *25*, 1270−1274.

(33) Dutta, S.; Ray, C.; Sarkar, S.; Pradhan, M.; Negishi, Y.; Pal, T. Silver Nanoparticle Decorated Reduced Graphene Oxide (rGO) Nanosheet: A Platform for SERS Based Low-Level Detection of Uranyl Ion. *ACS Appl. Mater. Interfaces* **2013**, *5*, 8724−8732.

(34) Xu, Z.; Cao, H.; Xin, H. Solution-Based Synthesis and Characterization of a Silver Nanoparticle−Graphene Hybrid Film. *Carbon* **2011**, *49*, 4731−4738.

(35) Xu, G.; Liu, J.; Wang, Q.; Hui, R.; Chen, Z.; Maroni, V. A.; Wu, J. Plasmonic Graphene Transparent Conductors. *Adv. Mater.* **2012**, *24*, OP71−OP76.

(36) Liu, X.; Cao, L.; Song, W.; Ai, K.; Lu, L. Functionalizing Metal Nanostructured Film with Graphene Oxide for Ultrasensitive Detection of Aromatic Molecules by Surface-Enhanced Raman Spectroscopy. *ACS Appl. Mater. Interfaces* **2011**, *3*, 2944−2952.

(37) Borini, S.; White, R.; Wei, D.; Astley, M.; Haque, S.; Spigone, E.; Harris, N.; Kivioja, J.; Ryhänen, T. Ultrafast Graphene Oxide Humidity Sensors. *ACS Nano* **2013**, *7*, 11166−11174.

(38) Han, T. H.; Huang, Y. K.; Tan, A. L.; Dravid, V.; Huang, J. Steam Etched Porous Graphene Oxide Network for Chemical Sensing. *J. Am. Chem. Soc.* **2011**, *133*, 15264−15267.
(39) Li, C.; Zhang, D.; Liu, X.; Han, S.; Tang, T.; Han, J.; Zhou, C. In_2O_3 Nanowires as Chemical Sensors. *Appl. Phys. Lett.* **2003**, *82*, 1613−1615.
(40) Xiong, W.; Kale, G. Novel High-Selectivity NO_2 Sensor for Sensing Low-Level NO_2. *Electrochem. Solid-State Lett.* **2005**, *8*, 49−53.
(41) Qin, Y.; Hu, M.; Zhang, J. Microstructure Characterization and NO_2-Sensing Properties of Tungsten Oxide Nanostructures. *Sens. Actuators, B* **2010**, *150*, 339−345.
(42) Bai, S.; Zhang, K.; Luo, R.; Li, D.; Chen, A.; Liu, C. C. Low-Temperature Hydrothermal Synthesis of WO_3 Nanorods and Their Sensing Properties for NO_2. *J. Mater. Chem.* **2012**, *22*, 12643−12650.
(43) Zhao, M.; Huang, J. X.; Ong, C. W. Diffusion-Controlled H_2 Sensors Composed of Pd-Coated Highly PorousWO_3 Nanocluster Films Meng. *Sens. Actuators, B* **2014**, *191*, 711−718.